

Bridging Distribution Gaps in Time Series Foundation Model Pretraining with Prototype-Guided Normalization

Peiliang Gong, Emadeldeen Eldele, Min Wu, *Senior Member, IEEE*, Zhenghua Chen, *Senior Member, IEEE*, Xiaoli Li, *Fellow, IEEE*, Daoqiang Zhang, *Senior Member, IEEE*

Abstract—Foundation models have achieved remarkable success across diverse machine-learning domains through large-scale pretraining on large, diverse datasets. However, pretraining on such datasets introduces significant challenges due to substantial mismatches in data distributions, a problem particularly pronounced with time series data. In this paper, we tackle this issue by proposing a domain-aware adaptive normalization strategy within the Transformer architecture. Specifically, we replace the traditional LayerNorm with a prototype-guided dynamic normalization mechanism (*ProtoNorm*), where learned prototypes encapsulate distinct data distributions, and sample-to-prototype affinity determines the appropriate normalization layer. This mechanism effectively captures the heterogeneity of time series characteristics, aligning pretrained representations with downstream tasks. Through comprehensive empirical evaluation, we demonstrate that our method significantly outperforms conventional pretraining techniques across both classification and forecasting tasks, while effectively mitigating the adverse effects of distribution shifts during pretraining. Incorporating *ProtoNorm* is as simple as replacing a single line of code. Extensive experiments on diverse real-world time series benchmarks validate the robustness and generalizability of our approach, advancing the development of more versatile time series foundation models.

Index Terms—Foundation Models, Pretraining, Time Series Analysis, Distribution Shift, Prototypical Learning

I. INTRODUCTION

FOUNDATION Models (FM) have revolutionized machine learning by learning general-purpose representations from vast amounts of unlabeled data [1]. These models have achieved remarkable success, particularly in natural language processing (NLP) tasks [2]. Prominent examples, such as GPT-3 [3], GPT-4 [4], and LLAMA [5], demonstrate exceptional performance and generalization capabilities, leveraging the intrinsic structures and patterns in textual data.

The potential of FMs to generalize across diverse domains holds immense promise for extending their efficacy to time series (TS) domains, such as finance [6], healthcare [7], and climate forecasting [8]. However, unlike NLP tasks, where data distributions exhibit relative consistency and models can effectively capture patterns and semantics, training FMs on TS data presents a significant challenge due to mismatched pretraining data distributions [9].

Peiliang Gong and Daoqiang Zhang are with the Key Laboratory of Brain-Machine Intelligence Technology, Ministry of Education, College of Artificial Intelligence, Nanjing University of Aeronautics and Astronautics, Nanjing 211106, China

Emadeldeen Eldele, Zhenghua Chen, and Xiaoli Li are with the Institute for Infocomm Research (I²R) and the Centre for Frontier AI Research (CFAR), Agency for Science, Technology and Research (A*STAR), Singapore

Min Wu is with the Institute for Infocomm Research (I²R), Agency for Science, Technology and Research (A*STAR), Singapore

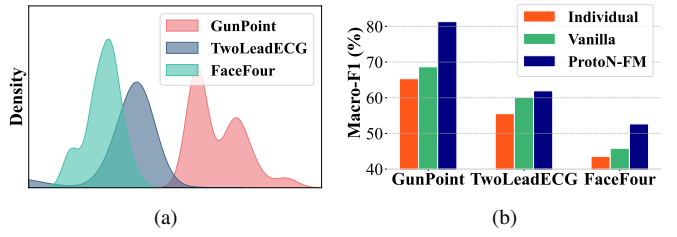


Fig. 1. (a) Distributional shifts exist among three UCR time series datasets. (b) Fine-tuning performance comparison on these datasets after different pretraining strategies. *Individual* refers to pretraining and fine-tuning a Transformer model on each dataset separately. *Vanilla* denotes pretraining the foundation model on multiple datasets without additional design considerations. In *ProtoN-FM*, we utilize the same multi-dataset pretraining, but incorporate our prototype-guided dynamic normalization mechanism, resulting in superior performance across diverse datasets.

This mismatch can be attributed to several factors. First, different TS data often manifest distinct properties, such as temporal dependencies, irregularities, and domain-specific dynamics. Second, TS data may exhibit varying sampling rates, number of channels, and noise levels, which deviate substantially from the clean and well-structured data employed in pretraining language models [10], [11]. To illustrate this disparity, Figure 1(a) depicts the distribution of different types of datasets (i.e., GunPoint, TwoLeadECG, and FaceFour) in the UCR classification archive. These datasets, originating from diverse domains, exhibit significant variations in their value ranges and morphological characteristics, underscoring the inherent heterogeneity present in TS data.

The implications of this distributional mismatch on pretraining FMs are demonstrated in Figure 1(b), which compares the fine-tuning performance across different pretraining strategies. The *Vanilla* pretraining strategy, which neglects dataset heterogeneity, yields suboptimal fine-tuning results. Conversely, strategies that address this mismatch during pretraining demonstrate superior performance, highlighting the criticality of aligning FMs with the intrinsic characteristics of TS data.

In this work, we propose a novel approach to address the discrepancy between FM pretraining and TS data distributions. Specifically, we introduce an FM design based on a **Prototype-guided dynamic Normalization (*ProtoNorm*)** mechanism within the Transformer architecture, enabling adaptive normalization tailored to the heterogeneous characteristics of TS data. As shown in Figure 2, the *ProtoNorm* mechanism operates by learning a set of prototypes during pretraining, where each prototype encapsulates a cluster of data with

shared attributes, such as temporal dependencies, noise levels, or sampling rates.

Unlike conventional LayerNorm, which applies fixed normalization parameters across all samples, our method assigns each prototype to its corresponding LayerNorm module, capturing the distinctive statistical properties of different data clusters. During training, the model computes an affinity score between each sample and the learned prototypes, dynamically selecting the most appropriate LayerNorm module based on the highest affinity. This adaptive selection process ensures that the normalization process aligns with the specific characteristics of each sample, effectively addressing the inherent heterogeneity in TS data.

Moreover, this adaptive mechanism integrates seamlessly within the Transformer architecture, leveraging its self-attention mechanism to further contextualize the prototype selection. By aligning the model's normalization process with the diverse characteristics of TS data, *ProtoNorm* mitigates the distribution shift during time series foundation model pretraining. This alignment enables the FM to generalize more effectively across domains and tasks, achieving superior fine-tuning performance and enhanced robustness compared to conventional approaches. The contributions of this work can be summarized as follows:

- This is the first work to identify the critical challenge of data distribution mismatch between foundation model pretraining and time series data, which impedes the effective deployment of FMs to time series tasks.
- We propose a prototype-guided dynamic normalization mechanism (*ProtoNorm*) that adaptively normalizes features based on learned distributional prototypes. This lightweight and modular solution integrates seamlessly into existing Transformer architectures to address distributional shifts during FM pretraining.
- Through comprehensive experiments across diverse time series tasks, including classification and forecasting, we demonstrate substantial improvements in both fine-tuning performance and generalization capabilities compared to conventional approaches, validating the efficacy of our distribution-aware learning paradigm.

II. RELATED WORK

A. Foundation Models for Time Series

Foundation models (FMs) have gained attention in TS analysis, following the success of Large Language Models (LLMs) in natural language processing (NLP) [11]. However, while some studies have adapted pretrained LLMs for TS data [12]–[15], this approach is not ideal for TS tasks. The inherent differences between text, which is discrete and categorical, and TS data, which is continuous and numeric, present significant challenges for LLM-based methods [16]. These models often fail to capture the unique temporal patterns and dynamics of TS data. Other research has focused on designing FMs specifically for TS tasks [17]–[19], often using self-supervised learning techniques like masked sequence prediction [20], [21], contrastive learning [22], [23], or hybrid methods [24], [25]. However, it's vital to distinguish works based on their

pretraining strategy. Some methods train on a single dataset and test on that same dataset, such as PatchTST [26] and TSLANet [27]. While these approaches can achieve strong performance within a specific domain, they do not involve pre-training on multiple datasets, limiting their ability to generalize across diverse TS domains. On the other hand, certain methods adopt a more generalizable approach by pretraining on a pool of datasets [16], [28], [29], aiming to build foundation models that can generalize well. However, even among these models, some fail to fully address the challenges posed by distribution shifts during pretraining, which can impact their efficacy in real-world applications across different domains.

B. Distribution Shifts in Time Series

Time series data is particularly prone to distribution shifts due to factors such as changes in sensor behavior, environmental variations, and temporal dynamics [30]. A growing body of research aims to mitigate these shifts in deep learning models through techniques such as domain adaptation [31]–[34] and domain generalization [35], [36]. These approaches seek to capture domain-invariant features that can be generalized across different distributions. Besides, architecture-specific mechanisms have been developed, including Adaptive RNNs [37], Non-stationary Transformers [38], Instance Normalization flows [39], [40], and contextualized adapters [41]. These mechanisms aim to alleviate the impact of non-stationary factors through distribution characterization. However, a significant drawback of these designs is their limited transferability across different model architectures, potentially hindering their broader applicability in diverse TS analysis scenarios. Beyond architecture-specific designs, several normalization-based strategies have been proposed to address distribution shifts in TS data [42], [43]. For instance, RevIN [9] introduced instance normalization to mitigate distribution shifts by leveraging statistics from individual samples to normalize TS data. Despite these advances, the application of such techniques to Transformer architectures remains limited, and their utilization in multi-dataset training scenarios is still underexplored.

C. Adaptive Normalization Techniques

Adaptive normalization methods, in contrast to traditional fixed schemes, learn flexible strategies to address covariate shift [44], [45]. For instance, Adaptive Batch Normalization dynamically adjusts normalization parameters across batches, while Adaptive Instance Normalization aligns channel-wise mean and variance to match style input [46]–[48]. Recent research has focused on developing adaptive normalization techniques specifically for the non-stationary characteristics of TS data [42], [49]. For example, DAIN introduced a non-linear network for adaptive input normalization [43], which was subsequently extended by various approaches [50], [51]. These extensions incorporated adaptive preprocessing layers into deep neural networks. RevIN proposed a symmetric, model-agnostic method that normalizes input sequences and denormalizes model output sequences in TS forecasting [9]. More recently, SAN introduced slice-level adaptive normalization, offering

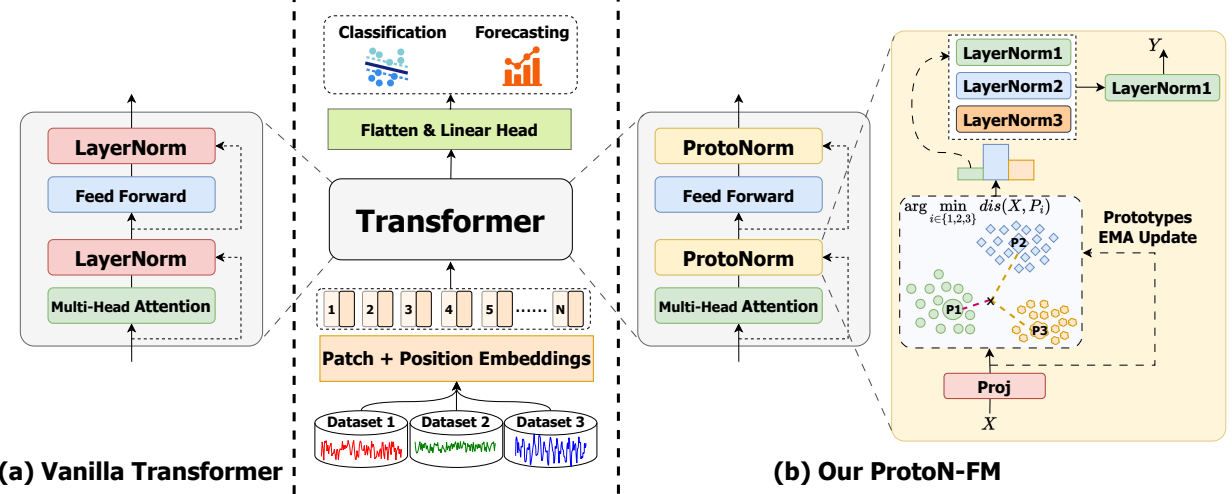


Fig. 2. Framework comparison between vanilla Transformer and our ProtoN-FM. (a) Vanilla Transformer with standard LayerNorm, employing fixed normalization parameters across all inputs. (b) Our ProtoN-FM with ProtoNorm mechanism for dynamic LayerNorm assignment via prototype-guided gating. Each input is assigned appropriate LayerNorm parameters based on its similarity to learned prototypes, where these prototypes undergo continuous refinement through EMA updates during training.

more flexible normalization and denormalization for TS forecasting [52], while SIN proposed selective and interpretable normalization to select statistics and learn the normalization transformation [53]. While existing normalization methods have shown efficacy, they assume uniform statistical properties across all TS instances, which may not be optimal while pretraining with multiple datasets. In contrast, we explicitly take the distribution inconsistencies into consideration during FM pretraining, offering a more nuanced and effective training strategy.

III. PROPOSED METHOD

A. Preliminaries

1) *Problem Definition*: Given a collection of time series datasets $\mathcal{D} = \{\mathcal{D}_k | k = 1, 2, \dots, n\}$, each dataset \mathcal{D}_k encompasses a variable number of samples with dimensions $L_k \times C_k$ (L_k denoting signal length and C_k representing the number of sensors or variables). Our objective is to pretrain a time series foundation model \mathcal{M} on this collection \mathcal{D} while addressing inter-dataset distributional shifts. The model subsequently undergoes fine-tuning on either a novel or known dataset utilizing limited data samples to achieve superior performance.

2) *Layer Normalization*: Layer Normalization (LN) [54] constitutes a fundamental training mechanism in deep learning networks, particularly in the prevalent Transformer architecture [55]. Unlike Batch Normalization (BN), which normalizes across the batch dimension, LN normalizes across features within a single layer. Analogous to BN, LN also incorporates two trainable affine parameters γ and β to enable network learning of distinct scales and shifts. Given a layer's activation $x \in \mathbb{R}^{C \times L}$ for a single input, LN is formulated as,

$$LN(x_i; \gamma, \beta) = \gamma \cdot \hat{x}_i + \beta, \quad (1)$$

where

$$\hat{x}_i = \frac{x_i - \mu}{\sqrt{\sigma^2 + \epsilon}}. \quad (2)$$

Here, μ denotes the mean and σ^2 represents the variance computed over layer features for a single input,

$$\mu = \frac{1}{d} \sum_{i=1}^d x_i, \quad \sigma^2 = \frac{1}{d} \sum_{i=1}^d (x_i - \mu)^2, \quad (3)$$

and ϵ is a small constant to prevent divide-by-zero.

During training, LN normalizes activations by computing mean and variance across features for each sample independently, mitigating internal covariate shift and enhancing training stability. During inference, LN executes identical normalization operations but with frozen parameters, implementing the learned scale and shift transformations. Unlike BN, LN's sample-wise normalization eschews running statistics, ensuring consistent behavior between training and inference.

B. Prototype-guided Dynamic Normalization Mechanism

It is important to explain why we chose to modify LN specifically, rather than other components of the Transformer, to address the distribution shift. LN is an ideal candidate for this modification because it has fewer parameters than other parts of the Transformer, making it computationally efficient to replicate. This allows us to handle variations across different datasets while minimizing the risk of overfitting.

Moreover, previous empirical evidence demonstrates that domain-specific normalization approaches, such as Batch-Norm, excel in mitigating domain shifts during adaptation tasks [47]. This insight motivated our development of a domain-aware normalization framework tailored for time series data. However, conventional LN approaches presume static relationship between input samples and their corresponding normalization strategies, potentially constraining the model's adaptability to both intra- and inter-dataset variations. Relying on a fixed normalization strategy across entire datasets may inadequately address challenges such as heterogeneous sample characteristics or cross-domain convergence.

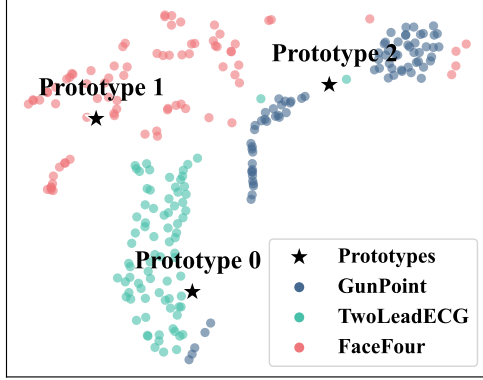


Fig. 3. Visualization of learned prototypes and sample features. Prototypes capture the unique distribution patterns of each cluster.

a) Prototype-Guided Gating Network: To overcome these limitations, we introduce ProtoN-FM, which implements an adaptive and dynamic normalization mechanism, as illustrated in Figure 2. Departing from fixed LN implementations per dataset, we propose *ProtoNorm* layer, comprising multiple LN modules, where selection occurs through a prototype-guided gating network that assigns each sample to its optimal LN based on prototype proximity. Post-pretraining, these learned prototypes function as distributional anchors, enabling sample-specific normalization strategy adaptation.

Figure 3 illustrates how learned prototypes function as distributional anchors, capturing distinct data distributions. This framework enables optimal normalization strategy selection per sample, accommodating both intra- and inter-dataset variations while enhancing the model's capacity to handle complex distributional overlaps.

Formally, each *ProtoNorm* layer incorporates n LayerNorm modules $\{LN_1, LN_2, \dots, LN_n\}$, alongside a prototypes-guided gating network \mathcal{G} . Considering a signal v with features x , \mathcal{G} determines the appropriate LayerNorm for normalization by computing distances between x and predefined prototypes $\{p_1, p_2, \dots, p_n\}$, where each prototype is associated with a specific LayerNorm module.

b) Adaptive Normalization: The network selects LayerNorm module LN_i whose prototype p_i minimizes the distance to x , implementing optimal normalization mapping. This selection is given by:

$$i^* = \arg \min_{i \in \{1, 2, \dots, n\}} d(x, p_i), \quad (4)$$

where $d(x, p_i)$ represents the distance metric (e.g., Euclidean distance) between x and prototype p_i .

c) Prototype Update: The prototypes evolve during training via Exponential Moving Average (EMA) [56], ensuring adaptive refinement based on distributional dynamics. Formally, the prototype p_i is updated as:

$$p_i^{(t+1)} = (1 - \alpha) \cdot p_i^{(t)} + \alpha \cdot x, \quad (5)$$

where $p_i^{(t)}$ denotes the prototype at time t , x represents the current cluster's input features, and α constitutes the EMA decay factor. This mechanism ensures continuous prototype refinement while maintaining distributional robustness.

d) Orthogonality Constraint: To maintain prototype distinctiveness, we incorporate an additional orthogonality constraint. The prototypes initialize with orthogonal parameters, facilitating enhanced discriminative capacity among diverse input features and distributions. Additionally, inspired by [57], we implement regularization to preserve prototype independence. Formally, given a matrix $P \in \mathbb{R}^{n \times d}$ where each row represents a prototype, the orthogonal loss is defined as:

$$\mathcal{L}_{\text{orth}} = \|PP^T - I\|_F^2, \quad (6)$$

where I is identity matrix, and $\|\cdot\|_F^2$ is Frobenius norm.

C. Self-supervised Pretraining Framework

Our pretraining framework employs augmentation-based contrastive learning for robust temporal representation acquisition. For input TS sample x , we apply two augmentation techniques: time-shift and scaling with jitter [22], generating two diverse views of the same sample, denoted as \tilde{x}_1 and \tilde{x}_2 . Time-shift augmentation introduces variations in signal timing by shifting the input sequence along the temporal axis, while scaling with jitter applies random scaling factors combined with small perturbations, simulating variability in signal amplitude and sensor noise.

The encoder and projector head transform \tilde{x}_1 and \tilde{x}_2 into representations z_1 and z_2 . We then utilize NT-Xent loss [58] to optimize view similarity while maintaining sample distinctiveness. For N -sample batches, the NT-Xent loss follows:

$$\mathcal{L}_{\text{NT-Xent}} = -\log \frac{\exp(\text{sim}(z_1, z_2)/\tau)}{\sum_{j=1}^{2N} \mathbf{1}_{[j \neq i]} \exp(\text{sim}(z_i, z_j)/\tau)}, \quad (7)$$

where $\text{sim}(z_1, z_2) = \frac{z_1 \cdot z_2}{\|z_1\| \|z_2\|}$ denotes the dot product between ℓ_2 normalized z_1 and z_2 (i.e., cosine similarity), τ represents temperature scaling, and $\mathbf{1}_{[j \neq i]}$ is an indicator function excluding the positive pair from the denominator.

The comprehensive pretraining objective integrates contrastive and orthogonal losses, ensuring robust representation learning and distinct, separable prototypes:

$$\mathcal{L} = \mathcal{L}_{\text{NT-Xent}} + \lambda \cdot \mathcal{L}_{\text{orth}}, \quad (8)$$

where λ is a hyperparameter that balances the contribution of the orthogonal loss, empirically set to 0.001 in our experiments.

D. Modular Design for Integration with Existing Models

Our *ProtoNorm* mechanism is designed as a modular component that can directly replace standard LN layers in existing Transformer-based architectures. This enables us to evaluate the impact of our normalization approach both as part of our complete pretraining framework and as a drop-in replacement in state-of-the-art models like MOMENT [20] and Moirai [28], without altering their original training objectives or architectures.

TABLE I

CLASSIFICATION RESULTS IN DIFFERENT DATASETS. RESULTS ARE AVERAGED ACROSS EACH SUBSET OF DATASETS. WE CALCULATE THE ACCURACY AND F1-SCORE (%) FOR EACH DATASET. **BLUE**: BEST RESULTS, **PURPLE**: SECOND BEST. FULL RESULTS ARE LISTED IN TABLES VI, IV, AND V IN APPENDIX.

Datasets	Accuracy				Macro-F1			
	Sup.	Individual	Vanilla	ProtoN-FM	Sup.	Individual	Vanilla	ProtoN-FM
UCR Archive (91 datasets)	62.03	61.53	66.66	67.78	48.30	47.65	52.50	53.51
Machine Fault Diagnosis (3 datasets)	50.58	56.17	66.30	70.33	46.88	54.03	61.95	67.13
Human Activity Recognition (5 datasets)	45.29	47.43	48.83	51.05	34.48	36.25	37.15	38.90
Average	52.63	55.04	60.60	63.05	43.22	45.98	50.53	53.18

IV. EXPERIMENTS

We conduct comprehensive evaluations to assess the efficacy of ProtoN-FM across time series classification and forecasting tasks. The detailed experimental results and comprehensive model analyses are provided in subsections A, B, and C in the Appendix.

A. Experimental Setup

a) Evaluation Strategy: Our validation framework employs a dual-pronged approach across time series domains. For classification, we evaluate the complete ProtoN-FM framework against established baselines with fine-tuning and assess ProtoNorm’s specific contribution through MOMENT [20] integration in zero-shot settings. For forecasting, we evaluate ProtoNorm’s effectiveness by incorporating it into Moirai [28] across both in-distribution and out-of-distribution scenarios. This approach isolates our normalization mechanism’s impact while demonstrating its broader applicability as a modular enhancement to foundation models.

b) Model Architecture and Integration: We adopt PatchTST [26] as our base architecture for its balanced performance and efficiency. The encoder adheres to standard Transformer design principles: patches undergo embedding transformation before processing through multiple layers of multi-head attention with ProtoNorm and feed-forward networks with subsequent ProtoNorm (Figure 2). Besides, to validate the effectiveness of our ProtoNorm, we integrate it into two recent representative foundation models—MOMENT [20] for classification and Moirai [28] for forecasting—while maintaining their original architectures and training protocols, only replacing their normalization layers with our prototype-guided mechanism. For computational efficiency and fair comparison, we utilize the small variants of both models (MOMENT_{small} and Moirai_{small}) in our experiments.

c) Handling Varying Time Series Characteristics: To address dataset heterogeneity, we implement standardized preprocessing across tasks. For variations in channel count, we employ channel replication from samples with fewer channels to achieve parity with the maximum channel count in the pretraining dataset ensemble, incorporating stochastic noise injection to mitigate overfitting risks. Regarding sequence length disparities, we utilize adaptive downsampling for extended sequences and zero-padding for truncated ones, standardizing to prescribed temporal dimensions: 512 timesteps for UCR

datasets, 1024 for MFD tasks, and 128 for HAR tasks. For MOMENT and Moirai baselines, we maintain their original preprocessing settings to ensure fair comparison. These techniques ensure consistent input dimensions while preserving data characteristics.

d) Hyperparameters: We optimize our model utilizing the AdamW optimizer with a learning rate of $1e-3$, weight decay of $1e-5$, and dropout rate of 0.15. A cosine learning rate scheduler with 2000 warmup steps is applied across all tasks. For UCR and MFD tasks, we use a pretraining batch size of 256 over 5 epochs, with embedding dimension of 256, 8 attention heads, 12 encoder layers, and patch size of 50. The input sequence length is set to 512 for UCR and 1024 for MFD tasks. Fine-tuning maintains this architecture but adjusts batch sizes to 32 for UCR and 64 for MFD tasks, extending training to 50 epochs. For HAR tasks, we use a pretraining batch size of 128 over 5 epochs, with embedding dimension of 128, 8 attention heads, 6 encoder layers, patch size of 32, and input sequence length of 128; fine-tuning reduces the batch size to 8 over 50 epochs. When comparing with MOMENT and Moirai baselines, we maintain their original hyperparameter settings. Model performance was evaluated using accuracy and macro-averaged F1 scores as primary metrics. Each experiment was repeated three times, with the average performance reported. Implementation uses PyTorch on NVIDIA L40 GPUs.

e) Data Preprocessing: We conduct comprehensive empirical evaluations across diverse time series domains, encompassing classification and forecasting tasks. For classification experiments, we leverage the 91 UCR archive datasets [59] with their predetermined train/test splits, further segmenting the training corpus into training (80%) and validation (20%) subsets. The model undergoes pretraining on the consolidated UCR collection prior to fine-tuning and evaluation on individual datasets. Notably, for baseline comparisons with MOMENT [20], we maintain methodological consistency with their experimental protocols. For MFD tasks, we augment the pretraining phase by incorporating three supplementary prognostics and health management (PHM) datasets: CWRU [60], FEMTO [61], and XJTUSY [62]. Subsequently, the model undergoes fine-tuning and evaluation on three target datasets (IMS [63], UO [64], and PU [65]). Analogously, for HAR tasks, we utilize five datasets (HHAR [66], SKODA [67], UCIHAR [68], USCHAD [69], and WISDM [70]) during pretraining, followed by individual dataset evaluation. Both MFD and HAR datasets, lacking predefined partitions, are

TABLE II

FORECASTING PERFORMANCE COMPARISON WITH DIFFERENT PREDICTION LENGTHS. RESULTS SHOW THE MEAN ABSOLUTE ERROR (MAE) AND MEAN SQUARED ERROR (MSE) METRICS FOR MOIRAI AND PROTON-FM MODELS ACROSS MULTIPLE BENCHMARKING DATASETS WITH DIFFERENT PREDICTION LENGTHS $\in \{96, 192, 336, 720\}$. **BLUE**: BEST RESULTS. THE RIGHTMOST COLUMNS SHOW AVERAGED PERFORMANCE ACROSS ALL PREDICTION LENGTHS.

Datasets	Metric	Prediction Length									
		96		192		336		720		Average	
		Moirai	ProtoN-FM	Moirai	ProtoN-FM	Moirai	ProtoN-FM	Moirai	ProtoN-FM	Moirai	ProtoN-FM
ETTh1	MAE	0.4033	0.4070	0.4209	0.4251	0.4314	0.4364	0.4473	0.4596	0.4257	0.4320
	MSE	0.3756	0.3747	0.4000	0.4005	0.4112	0.4146	0.4170	0.4332	0.4010	0.4058
ETTh2	MAE	0.3329	0.3334	0.3734	0.3729	0.3922	0.3879	0.4110	0.4105	0.3774	0.3762
	MSE	0.2868	0.2884	0.3487	0.3490	0.3709	0.3667	0.3848	0.3860	0.3478	0.3475
ETTm1	MAE	0.3681	0.3708	0.3820	0.3850	0.3962	0.3976	0.4187	0.4167	0.3913	0.3925
	MSE	0.3698	0.3684	0.3785	0.3829	0.3955	0.4027	0.4261	0.4291	0.3925	0.3958
ETTm2	MAE	0.2869	0.2781	0.3264	0.3181	0.3596	0.3569	0.4063	0.4141	0.3448	0.3418
	MSE	0.2135	0.2042	0.2768	0.2683	0.3304	0.3310	0.4047	0.4262	0.3064	0.3074
Electricity	MAE	0.2868	0.2799	0.2989	0.2906	0.3112	0.3027	0.3362	0.3288	0.3083	0.3005
	MSE	0.1948	0.1848	0.2106	0.1984	0.2247	0.2132	0.2582	0.2479	0.2221	0.2111
Weather	MAE	0.2126	0.2102	0.2493	0.2460	0.2817	0.2784	0.3210	0.3201	0.2662	0.2637
	MSE	0.1760	0.1729	0.2172	0.2118	0.2626	0.2560	0.3189	0.3171	0.2437	0.2395

systematically segmented into train/validation/test sets with a 60/20/20 ratio. For forecasting experiments, we strictly adhere to the experimental methodology of Moirai [28] to ensure fair comparison, encompassing their data preprocessing protocols, training paradigms, and evaluation metrics.

B. Classification Experiments

a) Datasets: We examine the classification efficacy of ProtoN-FM across 99 diverse datasets, encompassing 91 UCR Archive datasets [59], 3 machine fault diagnosis (MFD) datasets, and 5 human activity recognition (HAR) datasets. In particular, the MFD datasets include IMS [63], UO [64], and PU [65], while the HAR datasets consist of HHAR [66], SKODA [67], UCIHAR [68], USCHAD [69], and WISDM [70]. These datasets exhibit distinct characteristics and span a comprehensive range of time series applications. Detailed dataset descriptions are provided in supplementary material.

b) Baselines and Experimental Settings: We evaluate our method using PatchTST architecture [26] in both with and without fine-tuning settings. For evaluation with fine-tuning, we compare against supervised training (*Sup.*), individual dataset pretraining (*Individual*), and conventional multi-dataset pretraining (*Vanilla*). For MFD and HAR tasks, each utilizes 100 randomly sampled instances for fine-tuning, maintaining a minimum of 5 samples per class when required. For UCR Archive, we employ the complete training samples due to their constrained sample sizes and substantial variation in sample quantities across datasets. During fine-tuning, we substitute the self-supervised head with a linear classifier while maintaining frozen prototypes. For evaluation without fine-tuning, we benchmark against MOMENT [20] baseline by incorporating ProtoNorm into their framework. All evaluations employ held-out test sets.

c) Results with Fine-tuning: Table I demonstrates the consistent superiority of our ProtoN-FM method in time

series classification. Multi-dataset pretraining approaches exhibit substantial advantages, with vanilla pretraining attaining 60.60% average accuracy compared to 55.04% for individual pretraining and 52.63% for supervised learning. ProtoN-FM further elevates performance across all dataset categories. On UCR Archive, ProtoN-FM attains 67.78% accuracy and 53.51% Macro-F1, surpassing vanilla pretraining by 1.12% and 1.01% respectively. The improvements are more pronounced in MFD tasks (accuracy: 70.33% vs. 66.30%; Macro-F1: 67.13% vs. 61.95%) and remain consistent in HAR (51.05% accuracy, 38.90% Macro-F1). These empirical findings demonstrate that our prototype-guided normalization effectively mitigates distribution shifts while preserving robust generalization, achieving comprehensive averages of 63.05% accuracy and 53.18% Macro-F1 across diverse time series tasks.

d) Results without Fine-tuning: Figure 4(a) illustrates ProtoN-FM’s efficacy in classification without fine-tuning on UCR Archive. Employing an SVM classifier trained on learned representations, ProtoN-FM achieves 58.27% mean accuracy and 60.27% median accuracy, exceeding MOMENT baseline (57.70% mean, 59.42% median) by 0.57% and 0.85% respectively. This consistent improvement across both metrics indicates that our prototype-guided normalization mechanism facilitates more robust and transferable representations, even without task-specific adaptation. The superior performance in this challenging paradigm further substantiates our approach’s capability to effectively mitigate distribution shifts and extract generalizable patterns from time series data, rendering it particularly valuable in scenarios where labeled data is scarce or unavailable.

C. Forecasting Experiments

a) Datasets: To assess the efficacy of ProtoN-FM in forecasting tasks, we conduct extensive evaluations across 34 datasets, encompassing 28 datasets from the Monash Time

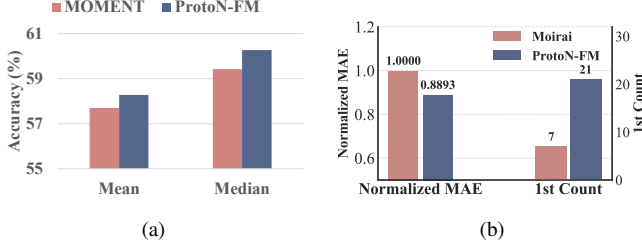


Fig. 4. Comparative analysis of model performance across classification and forecasting tasks. Full results are listed in Tables VII and VIII in Appendix. (a) Classification accuracy evaluation across 91 UCR datasets without fine-tuning. (b) Quantitative assessment via normalized MAE metrics and frequency of optimal performance on the Monash benchmark.

Series Forecasting Archive [71], and 6 datasets from a subset of the established long sequence forecasting benchmark [72], [73], comprising four ETT datasets (ETTh1, ETTh2, ETTm1, ETTm2), Electricity, and Weather dataset. Detailed dataset descriptions are provided in supplementary material.

b) Baselines and Experimental Settings: We evaluate our *ProtoNorm* through integration with Moirai [28] foundation model across both in-distribution (IID) and out-of-distribution (OOD) scenarios. For IID evaluation, we benchmark on Monash forecasting archive [71] utilizing normalized Mean Absolute Error (MAE) for direct comparison with Moirai baseline. For OOD evaluation, we examine model robustness on unseen datasets from a long sequence forecasting benchmark, employing both MSE and MAE metrics to quantify generalization capabilities across distribution shifts.

c) Results on In-distribution Forecasting: Figure 4(b) illustrates *ProtoN-FM*'s efficacy on the Monash Time Series Forecasting Benchmark. Our method achieves a normalized MAE of 0.8893, demonstrating an 11.07% enhancement over the Moirai baseline. Notably, *ProtoN-FM* exhibits superior performance at the individual dataset level, attaining optimal results on 21 datasets compared to Moirai's 7 datasets. This substantial performance differential (21 vs. 7) indicates that our prototype-guided normalization facilitates more robust and consistent forecasting capabilities across diverse time series distributions. These empirical findings substantiate our approach's efficacy in elevating foundation model performance for in-distribution forecasting tasks.

d) Results on Out-of-distribution Forecasting: Table II delineates OOD forecasting results across varying prediction lengths and datasets, demonstrating *ProtoN-FM*'s effectiveness. Our method exhibits particularly robust performance on the Electricity and Weather datasets, consistently surpassing Moirai across all prediction lengths in both metrics. Specifically, on the Electricity dataset, *ProtoN-FM* achieves systematic improvements with average MAE reduced from 0.3083 to 0.3005 and MSE from 0.2221 to 0.2111. The performance advantage persists across diverse prediction horizons, indicating robust long-term forecasting capabilities. For the ETT series datasets, the results exhibit mixed but generally competitive performance. While Moirai demonstrates marginal superiority on ETTh1 and ETTm1, *ProtoN-FM* exhibits enhanced performance on ETTh2 and ETTm2. Notably, on ETTm2, our method achieves substantial improvements for

TABLE III
ABLATION STUDY RESULTS ON MFD DATASETS SHOWING AVERAGE ACCURACY AND MACRO-F1 SCORES (%). **BLUE**: BEST.

Variants	Accuracy				Macro-F1			
	IMS	UO	PU	Avg	IMS	UO	PU	Avg
w/o ProtoGate	77.51	60.43	62.02	66.65	69.26	59.37	58.81	62.48
w/o Ortho	77.53	66.99	63.80	69.44	70.51	66.22	60.69	65.81
<i>ProtoN-FM</i>	78.78	68.56	63.65	70.33	73.03	67.93	60.43	67.13

shorter prediction lengths (96 and 192 steps), with MAE reduced from 0.2869 to 0.2781 and 0.3264 to 0.3181 respectively. This suggests our prototype-guided normalization mechanism excels at capturing local temporal patterns in specific data typologies. Furthermore, as prediction horizons increase, both models exhibit anticipated performance degradation, yet *ProtoN-FM* maintains its competitive advantage or demonstrates more graceful degradation, underscoring its robustness in challenging long-term forecasting scenarios.

V. MODEL ANALYSIS

A. Ablation Study

We conduct systematic ablation experiments to examine the contribution of each critical component within our model. Table III presents comparative analyses across MFD datasets, evaluating *ProtoN-FM* against two variants: w/o ProtoGate and w/o Ortho. The w/o ProtoGate variant implements domain-specific LayerNorm, substituting our prototype-guided gate network with dataset-specific LayerNorm selection (elaborated in the supplementary material). The w/o Ortho variant eliminates the orthogonality constraints from the prototype learning process. The empirical results substantiate the efficacy of our design choices. Removing the prototype-guided gate network (w/o ProtoGate) yields a substantial performance degradation, with average accuracy declining from 70.33% to 66.65% and Macro-F1 from 67.13% to 62.48%. This marked deterioration underscores the significance of dynamic distribution matching over static dataset-specific normalization. Similarly, the elimination of orthogonality constraints (w/o Ortho) results in diminished performance (69.44% accuracy, 65.81% Macro-F1), validating our hypothesis that maintaining prototype diversity through orthogonality constraints facilitates enhanced feature distribution differentiation.

B. Scaling Efficiency

We conduct comprehensive experiments to examine the scaling efficiency of *ProtoN-FM* through prototype quantity and pretraining dataset dimensionality. Figure 5(a) illustrates model performance across varying prototype counts $\{4, 8, 16, 32, 64\}$ on 91 UCR datasets. The empirical results demonstrate performance enhancement with increasing prototypes up to 32, attaining peak accuracy at 67.78%, followed by marginal degradation at 64 prototypes. This indicates that 32 prototypes establish an optimal balance between model capacity and performance, while further increases may induce potential overfitting. Figure 5(b) illustrates the impact of pretraining

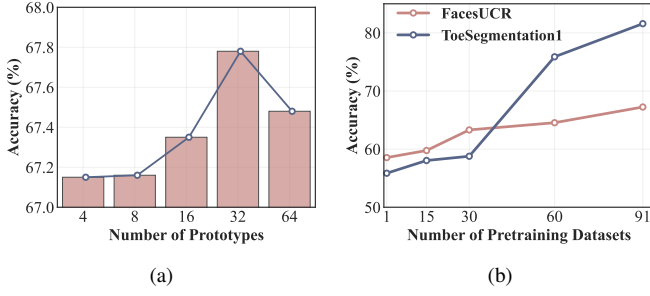


Fig. 5. Scaling efficiency analysis. (a) Average classification accuracy of ProtoN-FM across 91 UCR datasets with varying prototype quantities. Full results are listed in Table IX in Appendix. (b) Pretraining dataset scale’s impact on classification accuracy, evaluated across two UCR datasets.

dataset size on model efficacy, evaluated on two representative UCR datasets. Both exhibit consistent enhancement patterns with increasing pretraining datasets, albeit with distinct scaling characteristics. FacesUCR manifests steady progression from 58.54% to 67.24% accuracy, while ToeSegmentation1 demonstrates pronounced improvements, particularly in later stages, escalating from 55.85% to 81.58%. This substantial enhancement validates our model’s capacity to effectively leverages expanded pretraining data, substantiating the benefits of large-scale pretraining for time series foundation models.

These scaling analyses reveal that ProtoN-FM efficacy in capturing diverse temporal patterns with optimized prototype quantity while exhibiting robust scaling capabilities with augmented pretraining data, suggesting its potential for even larger-scale applications.

C. Complexity Analysis

We conduct a detailed analysis of our ProtoN-FM’s computational complexity versus baseline PatchTST, as illustrated in Figure 6, examining model parameters, classification accuracy, and computational requirements on the UCR GunPoint dataset. ProtoN-FM exhibits minimal parameter overhead: from PatchTST’s 7.91M parameters to 7.95M (ProtoN4-FM), 8.00M (ProtoN8-FM), 8.11M (ProtoN16-FM), 8.31M (ProtoN32-FM), and 8.72M (ProtoN64-FM), with maximum increase under 10%. Performance-wise, accuracy enhances significantly with increasing prototypes, with ProtoN32-FM attaining optimal accuracy at 81.33% (versus PatchTST’s 68.67%), representing a substantial 12.66% improvement. Accuracy demonstrates consistent ascension until 32 prototypes, before marginally declining to 78.44% with 64 prototypes. Notably, computational cost maintains 2.53 FLOPs across all prototype configurations, indicating negligible computational overhead from our prototype-guided normalization mechanism. This substantiates ProtoN-FM’s capability to achieve superior performance while preserving computational efficiency, establishing its practicality for real-world deployment.

D. Parameter Analysis on Orthogonal Weights

We conduct additional parameter analyses of orthogonal loss weight to further validate model robustness. These empirical

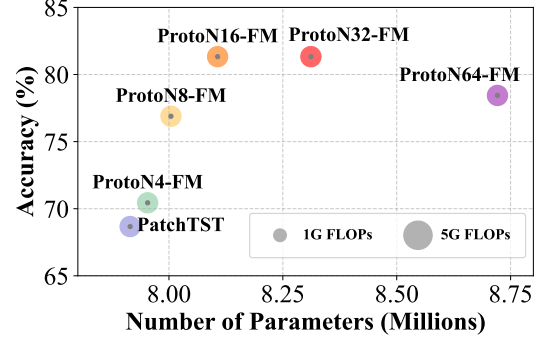


Fig. 6. Performance analysis of ProtoN-FM across varying prototype quantities versus baseline, examining parameter count and FLOPs on UCR GunPoint dataset.

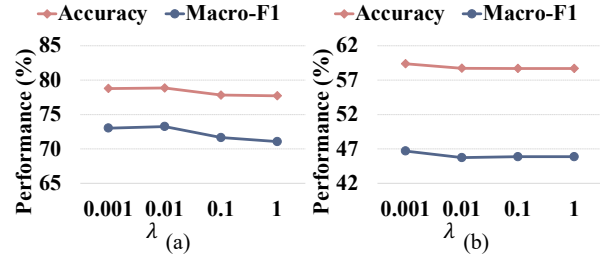


Fig. 7. Performance evaluation with varying λ parameters on representative datasets. (a) Mean performance metrics on IMS dataset (MFD task). (b) Mean performance metrics on UCIHAR dataset (HAR task).

investigations complement our primary analysis through examination of parameter sensitivity across diverse application domains. Figure 7 examines orthogonal loss weight $\lambda \in \{0.001, 0.01, 0.1, 1\}$ impact on IMS (MFD task) and UCIHAR (HAR task) datasets. For IMS, $\lambda = 0.01$ yields optimal efficacy with accuracy of 78.86% and Macro-F1 score of 73.25%. Performance degradation at higher λ values suggests potential over-regularization. Conversely, the UCIHAR dataset exhibits minimal sensitivity to λ variations, with peak accuracy of 59.38% and Macro-F1 of 46.69% are observed at $\lambda = 0.001$, maintaining performance stability across varying parameters. These empirical findings indicate robust model performance across λ configurations, with smaller values generally sufficient for optimal efficacy.

E. Distribution Shift Analysis

We examine ProtoN-FM’s robustness under varying levels of distribution shifts utilizing the IMS dataset. We generate three synthetic variants (IMS-N1, IMS-N2, IMS-N3) by introducing Gaussian noise with increasing standard deviations (0.1, 0.2, and 0.3, respectively). The model undergoes pretraining on paired datasets (IMS with IMS-N1, IMS-N2, or IMS-N3) followed by fine-tuning on a constrained IMS subset. Figure 8 illustrates comparative performance between ProtoN-FM and vanilla pretraining approach across perturbation scenarios. The empirical results demonstrate ProtoN-FM’s consistent superiority, particularly in the most challenging scenario (IMS-N3), where it enhances accuracy from 67.05% to 70.54% and Macro-F1 from 63.84% to

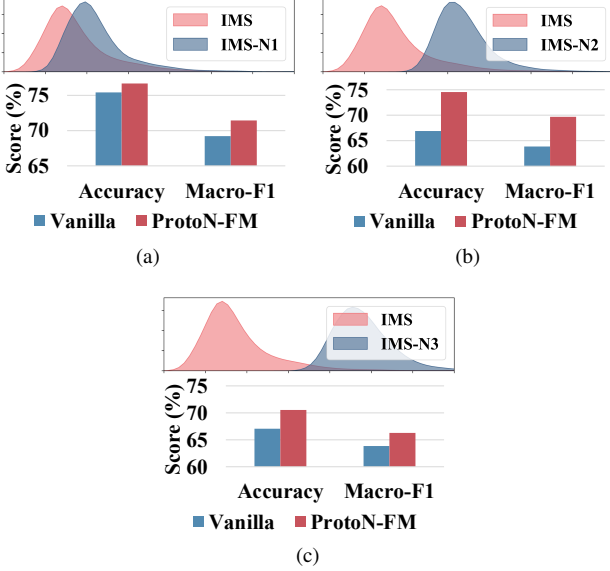


Fig. 8. Performance analysis under varying distribution shifts. Comparative evaluation of ProtoN-FM versus vanilla pretraining on IMS, where (a), (b), and (c) represent pretraining scenarios with progressively perturbed IMS variants (IMS-N1, IMS-N2, IMS-N3), followed by fine-tuning and evaluation on original IMS data.

66.28%. These substantial performance gains substantiate our prototype-guided normalization strategy’s efficacy in mitigating distribution shifts.

VI. CONCLUSION

This paper introduces ProtoN-FM, a novel approach addressing distributional discrepancies between foundation model pretraining and time series data. ProtoN-FM facilitates adaptive normalization through prototype-based similarity assessment. Unlike conventional LayerNorm’s fixed normalization parameters, our approach learns distinctive prototypes capturing diverse data characteristics, each coupled with a specialized LayerNorm module. Through comprehensive empirical evaluation across time series tasks, we demonstrate ProtoN-FM’s consistent superiority over traditional approaches, particularly under significant distribution shifts. Future research directions encompass exploring universal capabilities across additional downstream tasks and integrating ProtoNorm into diverse Transformer architectures to maximize its pretraining potential.

REFERENCES

- [1] C. Zhou, Q. Li, C. Li, J. Yu, Y. Liu, G. Wang, K. Zhang, C. Ji, Q. Yan, L. He *et al.*, “A comprehensive survey on pretrained foundation models: A history from bert to chatgpt,” *arXiv preprint arXiv:2302.09419*, 2023.
- [2] J. D. M.-W. C. Kenton and L. K. Toutanova, “Bert: Pre-training of deep bidirectional transformers for language understanding,” in *Proceedings of naacl-HLT*, vol. 1. Minneapolis, Minnesota, 2019, p. 2.
- [3] T. B. Brown, “Language models are few-shot learners,” *arXiv preprint arXiv:2005.14165*, 2020.
- [4] J. Achiam, S. Adler, S. Agarwal, L. Ahmad, I. Akkaya, F. L. Aleman, D. Almeida, J. Altenschmidt, S. Altman, S. Anadkat *et al.*, “Gpt-4 technical report,” *arXiv preprint arXiv:2303.08774*, 2023.
- [5] H. Touvron, T. Lavril, G. Izacard, X. Martinet, M.-A. Lachaux, T. Lacroix, B. Rozière, N. Goyal, E. Hambro, F. Azhar *et al.*, “Llama: Open and efficient foundation language models,” *arXiv preprint arXiv:2302.13971*, 2023.
- [6] X. Yu, Z. Chen, Y. Ling, S. Dong, Z. Liu, and Y. Lu, “Temporal data meets llm-explainable financial time series forecasting,” *arXiv preprint arXiv:2306.11025*, 2023.
- [7] M. Moor, O. Banerjee, Z. S. H. Abad, H. M. Krumholz, J. Leskovec, E. J. Topol, and P. Rajpurkar, “Foundation models for generalist medical artificial intelligence,” *Nature*, vol. 616, no. 7956, pp. 259–265, 2023.
- [8] H. Wu, H. Zhou, M. Long, and J. Wang, “Interpretable weather forecasting for worldwide stations with a unified deep model,” *Nature Machine Intelligence*, vol. 5, no. 6, pp. 602–611, 2023.
- [9] T. Kim, J. Kim, Y. Tae, C. Park, J.-H. Choi, and J. Choo, “Reversible instance normalization for accurate time-series forecasting against distribution shift,” in *International Conference on Learning Representations*, 2021.
- [10] Y. Wang, H. Wu, J. Dong, Y. Liu, M. Long, and J. Wang, “Deep time series models: A comprehensive survey and benchmark,” *arXiv preprint arXiv:2407.13278*, 2024.
- [11] Y. Liang, H. Wen, Y. Nie, Y. Jiang, M. Jin, D. Song, S. Pan, and Q. Wen, “Foundation models for time series analysis: A tutorial and survey,” in *Proceedings of the 30th ACM SIGKDD Conference on Knowledge Discovery and Data Mining*, 2024, pp. 6555–6565.
- [12] D. Cao, F. Jia, S. O. Arik, T. Pfister, Y. Zheng, W. Ye, and Y. Liu, “Tempo: Prompt-based generative pre-trained transformer for time series forecasting,” *arXiv preprint arXiv:2310.04948*, 2023.
- [13] K. Rasul, A. Ashok, A. R. Williams, H. Ghonia, R. Bhagwatkar, A. Khorasani, M. J. D. Bayazi, G. Adamopoulos, R. Riachi, N. Hassen, M. Biloš, S. Garg, A. Schneider, N. Chapados, A. Drouin, V. Zantedeschi, Y. Nevmyvaka, and I. Rish, “Lag-llama: Towards foundation models for probabilistic time series forecasting,” 2024.
- [14] S. Gao, T. Koker, O. Queen, T. Hartvigsen, T. Tsilgkardis, and M. Zitnik, “Units: Building a unified time series model,” *arXiv*, 2024.
- [15] T. Zhou, P. Niu, X. Wang, L. Sun, and R. Jin, “One fits all: Power general time series analysis by pretrained LM,” in *Advances in Neural Information Processing Systems 36: Annual Conference on Neural Information Processing Systems 2023, NeurIPS 2023, New Orleans, LA, USA, December 10 - 16, 2023*, 2023.
- [16] J. Li, J. Peng, H. Li, and L. Chen, “Unicl: A universal contrastive learning framework for large time series models,” *arXiv preprint arXiv:2405.10597*, 2024.
- [17] A. Das, W. Kong, R. Sen, and Y. Zhou, “A decoder-only foundation model for time-series forecasting,” in *Forty-first International Conference on Machine Learning, ICML 2024, Vienna, Austria, July 21-27, 2024*. OpenReview.net, 2024.
- [18] Y. Liu, H. Zhang, C. Li, X. Huang, J. Wang, and M. Long, “Timer: Generative pre-trained transformers are large time series models,” in *Forty-first International Conference on Machine Learning*, 2024.
- [19] J. Dong, H. Wu, Y. Wang, Y. Qiu, L. Zhang, J. Wang, and M. Long, “Timesiam: A pre-training framework for siamese time-series modeling,” in *ICML*, 2024.
- [20] M. Goswami, K. Szafer, A. Choudhry, Y. Cai, S. Li, and A. Dubrawski, “MOMENT: A family of open time-series foundation models,” in *Forty-first International Conference on Machine Learning, ICML 2024, Vienna, Austria, July 21-27, 2024*. OpenReview.net, 2024.
- [21] Z. Li, Z. Rao, L. Pan, P. Wang, and Z. Xu, “Ti-mae: Self-supervised masked time series autoencoders,” *arXiv preprint arXiv:2301.08871*, 2023.
- [22] E. Eldele, M. Ragab, Z. Chen, M. Wu, C.-K. Kwok, X. Li, and C. Guan, “Self-supervised contrastive representation learning for semi-supervised time-series classification,” *IEEE Transactions on Pattern Analysis and Machine Intelligence*, 2023.
- [23] C.-C. M. Yeh, X. Dai, H. Chen, Y. Zheng, Y. Fan, A. Der, V. Lai, Z. Zhuang, J. Wang, L. Wang *et al.*, “Toward a foundation model for time series data,” in *Proceedings of the 32nd ACM International Conference on Information and Knowledge Management*, 2023, pp. 4400–4404.
- [24] S. Lee, T. Park, and K. Lee, “Learning to embed time series patches independently,” in *The Twelfth International Conference on Learning Representations, ICLR 2024, Vienna, Austria, May 7-11, 2024*. OpenReview.net, 2024.
- [25] J. Dong, H. Wu, H. Zhang, L. Zhang, J. Wang, and M. Long, “Simmtm: A simple pre-training framework for masked time-series modeling,” *Advances in Neural Information Processing Systems*, vol. 36, 2024.
- [26] Y. Nie, N. H. Nguyen, P. Sinthong, and J. Kalagnanam, “A time series is worth 64 words: Long-term forecasting with transformers,” in *International Conference on Learning Representations*, 2023.
- [27] E. Eldele, M. Ragab, Z. Chen, M. Wu, and X. Li, “Tslanet: Rethinking transformers for time series representation learning,” in *International Conference on Machine Learning*, 2024.

[28] G. Woo, C. Liu, A. Kumar, C. Xiong, S. Savarese, and D. Sahoo, “Unified training of universal time series forecasting transformers,” in *Forty-first International Conference on Machine Learning, ICML 2024, Vienna, Austria, July 21-27, 2024*. OpenReview.net, 2024.

[29] A. F. Ansari, L. Stella, C. Turkmen, X. Zhang, P. Mercado, H. Shen, O. Shchur, S. S. Rangapuram, S. Pineda Arango, S. Kapoor, J. Zschiegner, D. C. Maddix, H. Wang, M. W. Mahoney, K. Torkkola, A. Gordon Wilson, M. Bohlke-Schneider, and Y. Wang, “Chronos: Learning the language of time series,” *arXiv preprint arXiv:2403.07815*, 2024.

[30] D. Akay and M. Atak, “Grey prediction with rolling mechanism for electricity demand forecasting of turkey,” *energy*, vol. 32, no. 9, pp. 1670–1675, 2007.

[31] M. Ragab, E. Eldele, W. L. Tan, C.-S. Foo, Z. Chen, M. Wu, C.-K. Kwoh, and X. Li, “Adatime: A benchmarking suite for domain adaptation on time series data,” *ACM Transactions on Knowledge Discovery from Data*, vol. 17, no. 8, pp. 1–18, 2023.

[32] H. He, O. Queen, T. Koker, C. Cuevas, T. Tsiligkaridis, and M. Zitnik, “Domain adaptation for time series under feature and label shifts,” in *International Conference on Machine Learning*. PMLR, 2023, pp. 12 746–12 774.

[33] P. Gong, M. Ragab, E. Eldele, W. Zhang, M. Wu, C.-S. Foo, D. Zhang, X. Li, and Z. Chen, “Evidentially calibrated source-free time-series domain adaptation with temporal imputation,” *arXiv preprint arXiv:2406.02635*, 2024.

[34] F. Ott, D. Rügamer, L. Heublein, B. Bischl, and C. Mutschler, “Domain adaptation for time-series classification to mitigate covariate shift,” in *Proceedings of the 30th ACM international conference on multimedia*, 2022, pp. 5934–5943.

[35] S. Deng, O. Sprangers, M. Li, S. Schelter, and M. de Rijke, “Domain generalization in time series forecasting,” *ACM Transactions on Knowledge Discovery from Data*, vol. 18, no. 5, pp. 1–24, 2024.

[36] W. Lu, J. Wang, X. Sun, Y. Chen, X. Ji, Q. Yang, and X. Xie, “Diversify: A general framework for time series out-of-distribution detection and generalization,” *IEEE Transactions on Pattern Analysis and Machine Intelligence*, vol. 46, no. 6, pp. 4534–4550, 2024.

[37] Y. Du, J. Wang, W. Feng, S. Pan, T. Qin, R. Xu, and C. Wang, “Adarnn: Adaptive learning and forecasting of time series,” in *Proceedings of the 30th ACM international conference on information & knowledge management*, 2021, pp. 402–411.

[38] Y. Liu, H. Wu, J. Wang, and M. Long, “Non-stationary transformers: Exploring the stationarity in time series forecasting,” *Advances in Neural Information Processing Systems*, vol. 35, pp. 9881–9893, 2022.

[39] W. Fan, P. Wang, D. Wang, D. Wang, Y. Zhou, and Y. Fu, “Dish-ts: a general paradigm for alleviating distribution shift in time series forecasting,” in *Proceedings of the AAAI conference on artificial intelligence*, vol. 37, no. 6, 2023, pp. 7522–7529.

[40] W. Fan, S. Zheng, P. Wang, R. Xie, J. Bian, and Y. Fu, “Addressing distribution shift in time series forecasting with instance normalization flows,” *arXiv preprint arXiv:2401.16777*, 2024.

[41] M. Chen, L. Shen, H. Fu, Z. Li, J. Sun, and C. Liu, “Calibration of time-series forecasting: Detecting and adapting context-driven distribution shift,” in *Proceedings of the 30th ACM SIGKDD Conference on Knowledge Discovery and Data Mining*, 2024, pp. 341–352.

[42] E. Ogasawara, L. C. Martinez, D. De Oliveira, G. Zimbrão, G. L. Pappa, and M. Mattoso, “Adaptive normalization: A novel data normalization approach for non-stationary time series,” in *The 2010 International Joint Conference on Neural Networks (IJCNN)*. IEEE, 2010, pp. 1–8.

[43] N. Passalis, A. Tefas, J. Kanniainen, M. Gabbouj, and A. Iosifidis, “Deep adaptive input normalization for time series forecasting,” *IEEE transactions on neural networks and learning systems*, vol. 31, no. 9, pp. 3760–3765, 2019.

[44] M. G. Vivek Panday, Rajesh Wadhvani, “Selective review on adaptive normalization techniques,” in *Proceedings of the Workshop on Intelligent Systems (WINS 2022)*, 2022, pp. 51–59.

[45] X. Fan, Q. Wang, J. Ke, F. Yang, B. Gong, and M. Zhou, “Adversarially adaptive normalization for single domain generalization,” in *Proceedings of the IEEE/CVF conference on Computer Vision and Pattern Recognition*, 2021, pp. 8208–8217.

[46] Y. Li, N. Wang, J. Shi, X. Hou, and J. Liu, “Adaptive batch normalization for practical domain adaptation,” *Pattern Recognition*, vol. 80, pp. 109–117, 2018.

[47] W.-G. Chang, T. You, S. Seo, S. Kwak, and B. Han, “Domain-specific batch normalization for unsupervised domain adaptation,” in *Proceedings of the IEEE/CVF conference on Computer Vision and Pattern Recognition*, 2019, pp. 7354–7362.

[48] E. S. Lubana, R. Dick, and H. Tanaka, “Beyond batchnorm: Towards a unified understanding of normalization in deep learning,” *Advances in Neural Information Processing Systems*, vol. 34, pp. 4778–4791, 2021.

[49] J. Deng, X. Chen, R. Jiang, X. Song, and I. W. Tsang, “St-norm: Spatial and temporal normalization for multi-variate time series forecasting,” in *Proceedings of the 27th ACM SIGKDD conference on knowledge discovery & data mining*, 2021, pp. 269–278.

[50] D. T. Tran, J. Kanniainen, M. Gabbouj, and A. Iosifidis, “Data normalization for bilinear structures in high-frequency financial time-series,” in *2020 25th International Conference on Pattern Recognition (ICPR)*. IEEE, 2021, pp. 7287–7292.

[51] M. A. September, F. S. Passino, L. Goldmann, and A. Hinel, “Extended deep adaptive input normalization for preprocessing time series data for neural networks,” in *AISTATS*, 2024, pp. 1891–1899.

[52] Z. Liu, M. Cheng, Z. Li, Z. Huang, Q. Liu, Y. Xie, and E. Chen, “Adaptive normalization for non-stationary time series forecasting: A temporal slice perspective,” *Advances in Neural Information Processing Systems*, vol. 36, 2024.

[53] L. Han, H.-J. Ye, and D.-C. Zhan, “Sin: Selective and interpretable normalization for long-term time series forecasting,” in *Forty-first International Conference on Machine Learning*.

[54] J. L. Ba, J. R. Kiros, and G. E. Hinton, “Layer normalization,” 2016. [Online]. Available: <https://arxiv.org/abs/1607.06450>

[55] A. Vaswani, “Attention is all you need,” *Advances in Neural Information Processing Systems*, 2017.

[56] D. P. Kingma, “Adam: A method for stochastic optimization,” *arXiv preprint arXiv:1412.6980*, 2014.

[57] K. Saito, Y. Ushiku, and T. Harada, “Asymmetric tri-training for unsupervised domain adaptation,” in *International conference on machine learning*. PMLR, 2017, pp. 2988–2997.

[58] T. Chen, S. Kornblith, M. Norouzi, and G. Hinton, “A simple framework for contrastive learning of visual representations,” in *International conference on machine learning*. PMLR, 2020, pp. 1597–1607.

[59] H. A. Dau, A. Bagnall, K. Kamgar, C.-C. M. Yeh, Y. Zhu, S. Gharghabi, C. A. Ratanamahatana, and E. Keogh, “The ucr time series archive,” *IEEE/CAA Journal of Automatica Sinica*, vol. 6, no. 6, pp. 1293–1305, 2019.

[60] W. A. Smith and R. B. Randall, “Rolling element bearing diagnostics using the case western reserve university data: A benchmark study,” *Mechanical systems and signal processing*, vol. 64, pp. 100–131, 2015.

[61] P. Nectoux, R. Gouriveau, K. Medjaher, E. Ramasso, B. Chebel-Morello, N. Zerhouni, and C. Varnier, “Pronostia: An experimental platform for bearings accelerated degradation tests,” in *IEEE International Conference on Prognostics and Health Management, PHM’12*. IEEE Catalog Number: CP12PHM-CDR, 2012, pp. 1–8.

[62] B. Wang, Y. Lei, N. Li, and N. Li, “A hybrid prognostics approach for estimating remaining useful life of rolling element bearings,” *IEEE Transactions on Reliability*, vol. 69, no. 1, pp. 401–412, 2020.

[63] H. Qiu, J. Lee, J. Lin, and G. Yu, “Wavelet filter-based weak signature detection method and its application on rolling element bearing prognostics,” *Journal of sound and vibration*, vol. 289, no. 4–5, pp. 1066–1090, 2006.

[64] H. Huang and N. Baddour, “Bearing vibration data collected under time-varying rotational speed conditions,” *Data in brief*, vol. 21, pp. 1745–1749, 2018.

[65] C. Lessmeier, J. K. Kimotho, D. Zimmer, and W. Sextro, “Condition monitoring of bearing damage in electromechanical drive systems by using motor current signals of electric motors: A benchmark data set for data-driven classification,” in *PHM Society European Conference*, vol. 3, no. 1, 2016.

[66] A. Stisen, H. Blunck, S. Bhattacharya, T. S. Prentow, M. B. Kjærgaard, A. Dey, T. Sonne, and M. M. Jensen, “Smart devices are different: Assessing and mitigating mobile sensing heterogeneities for activity recognition,” in *Proceedings of the 13th ACM conference on embedded networked sensor systems*, 2015, pp. 127–140.

[67] T. Stiefmeier, D. Roggen, G. Ogris, P. Lukowicz, and G. Tröster, “Wearable activity tracking in car manufacturing,” *IEEE Pervasive Computing*, vol. 7, no. 2, pp. 42–50, 2008.

[68] D. Anguita, A. Ghio, L. Oneto, X. Parra, J. L. Reyes-Ortiz *et al.*, “A public domain dataset for human activity recognition using smartphones,” in *Esann*, vol. 3, 2013, p. 3.

[69] M. Zhang and A. A. Sawchuk, “Usc-had: A daily activity dataset for ubiquitous activity recognition using wearable sensors,” in *Proceedings of the 2012 ACM conference on ubiquitous computing*, 2012, pp. 1036–1043.

- [70] J. R. Kwapisz, G. M. Weiss, and S. A. Moore, “Activity recognition using cell phone accelerometers,” *ACM SigKDD Explorations Newsletter*, vol. 12, no. 2, pp. 74–82, 2011.
- [71] R. Godahewa, C. Bergmeir, G. I. Webb, R. J. Hyndman, and P. Montero-Manso, “Monash time series forecasting archive,” *arXiv preprint arXiv:2105.06643*, 2021.
- [72] G. Lai, W.-C. Chang, Y. Yang, and H. Liu, “Modeling long-and short-term temporal patterns with deep neural networks,” in *The 41st international ACM SIGIR conference on research & development in information retrieval*, 2018, pp. 95–104.
- [73] H. Wu, J. Xu, J. Wang, and M. Long, “Autoformer: Decomposition transformers with auto-correlation for long-term series forecasting,” *Advances in neural information processing systems*, vol. 34, pp. 22419–22430, 2021.

APPENDIX

A. Classification Detailed Results

1) Full Results with Fine-tuning Experiments:

a) *Performance Comparison on MFD Task:* Table IV demonstrates the superiority of the proposed ProtoN-FM compared to three baseline approaches in MFD tasks. ProtoN-FM outperforms all other methods, achieving an average accuracy of 70.33% and an average Macro-F1 score of 67.13%. Notably, all self-supervised learning pretraining methods surpass supervised training, underscoring their capacity to capture intricate temporal patterns and variations inherent in time series data, thereby enabling enriched feature representations. Furthermore, multi-dataset pretraining exhibits enhanced efficacy compared to individual dataset pretraining, suggesting that the incorporation of diverse data facilitates more robust representation learning. While the Vanilla method demonstrates improvement over individual pretraining, it fails to account for distribution shifts between datasets, constraining its performance relative to ProtoN-FM. This empirical evidence validates that through explicit mitigation of these shifts via a prototype-guided dynamic normalization mechanism, ProtoN-FM effectively aligns its learning paradigm with the inherent heterogeneity present in real-world time series data.

b) *Performance Comparison on HAR Task:* Table V presents a comprehensive analysis of classification performance across HAR tasks. The proposed ProtoN-FM demonstrates exceptional efficacy relative to baseline approaches, achieving optimal performance metrics with a mean accuracy of 51.05% and Macro-F1 score of 38.90%. Consistent with observations from MFD tasks, all self-supervised learning pretraining paradigms surpass supervised training protocols. ProtoN-FM consistently outperforms the Vanilla approach, which, despite exhibiting improvements over individual pretraining, fails to adequately address inter-dataset distribution shifts. This empirical evidence underscores the significance of incorporating heterogeneous training data and accounting for the inherent variability in real-world HAR applications. These quantitative metrics validate that ProtoN-FM not only enhances classification accuracy but also facilitates a more sophisticated understanding of the underlying temporal dynamics in HAR domains.

c) *Performance Comparison on UCR Datasets:* Our empirical analysis on the UCR archive demonstrates the consistent superiority of ProtoN-FM across diverse time series classification tasks. Analyzing Table VI, we observe that

both vanilla pretraining and ProtoN-FM significantly outperform supervised learning (62.03% accuracy) and individual dataset pretraining (61.53% accuracy), validating the efficacy of multi-dataset pretraining paradigms. ProtoN-FM achieves the highest average accuracy of 67.78% and Macro-F1 of 53.51%, surpassing vanilla pretraining by 1.12% and 1.01% respectively. The effectiveness of ProtoN-FM is further substantiated by its predominance in performance rankings - attaining superior results across 42 datasets for accuracy and 41 datasets for Macro-F1, significantly exceeding vanilla pretraining’s achievements on 28 and 24 datasets respectively. Notably, ProtoN-FM demonstrates remarkable performance gains on challenging datasets like ToeSegmentation2 (69.49% vs 57.95% accuracy), FaceFour (58.71% vs 45.83% accuracy), and TwoPatterns (85.56% vs 79.96% accuracy). This consistent performance superiority across diverse datasets validates our prototype-guided normalization strategy’s efficacy in mitigating distribution shifts and capturing dataset-specific characteristics.

2) Full Results without Fine-tuning Experiments:

a) *Performance Comparison with MOMENT:* Through analysis of Table VII, we evaluate zero-shot classification efficacy without fine-tuning utilizing an SVM classifier trained on learned representations. ProtoN-FM demonstrates superior performance over MOMENT with enhanced mean accuracy (58.27% vs 57.70%) across 91 UCR datasets. Notably, ProtoN-FM achieves predominant performance on 55 out of 91 datasets, validating its efficacy in learning transferable representations. Significant performance gains are observed on challenging datasets including DiatomSizeReduction (78.43% vs 69.93%), Lightning7 (60.27% vs 52.05%), and ArrowHead (53.71% vs 40.57%). These empirical findings substantiate that our prototype-guided normalization mechanism enhances the model’s capacity to extract discriminative features without task-specific fine-tuning, particularly benefiting datasets exhibiting complex temporal dynamics.

B. Forecasting Detailed Results

1) *Full Results on In-distribution Forecasting Experiments:* Analyzing Table VIII, our ProtoN-FM demonstrates superior performance on the Monash Time Series Forecasting Benchmark compared to Moirai. With normalized MAE reduced from 1.0 to 0.8893, ProtoN-FM achieves an 11.07% improvement in overall forecasting accuracy. More significantly, ProtoN-FM achieves the best performance on 21 out of 28 datasets, compared to Moirai’s 7 datasets, indicating consistent superiority across diverse time series domains. Notable improvements are observed on complex datasets such as fred_md (4212.26 vs 6556.77), australian_electricity (238.80 vs 295.07), and us_births (570.33 vs 690.98), demonstrating ProtoN-FM’s effectiveness in handling various temporal patterns. The substantial performance gains across different types of time series data, from financial indicators to energy consumption patterns, validate our prototype-guided normalization mechanism’s ability to adapt to diverse data distributions in real-world forecasting scenarios.

TABLE IV

DETAILED PERFORMANCE COMPARISON OF VARIOUS METHODS ON MFD DATASETS. WE CALCULATE THE ACCURACY AND F1-SCORE (%) FOR EACH DATASET. **BLUE**: BEST, **PURPLE**: SECOND BEST.

Datasets	Accuracy				Macro-F1			
	Sup.	Individual	Vanilla	ProtoN-FM	Sup.	Individual	Vanilla	ProtoN-FM
IMS	54.22	59.48	<u>77.00</u>	78.78	47.84	57.79	<u>68.39</u>	73.03
UO	49.32	50.62	<u>60.00</u>	68.56	48.20	49.33	<u>58.81</u>	67.93
PU	48.19	58.42	<u>61.91</u>	63.65	44.61	54.98	<u>58.66</u>	60.43
Average	50.58	56.17	<u>66.30</u>	70.33	46.88	54.03	<u>61.95</u>	67.13

TABLE V

DETAILED PERFORMANCE COMPARISON OF VARIOUS METHODS ON HAR DATASETS. WE CALCULATE THE ACCURACY AND F1-SCORE (%) FOR EACH DATASET. **BLUE**: BEST, **PURPLE**: SECOND BEST.

Datasets	Accuracy				Macro-F1			
	Sup.	Individual	Vanilla	ProtoN-FM	Sup.	Individual	Vanilla	ProtoN-FM
HHAR	69.57	70.23	<u>71.07</u>	72.43	61.44	62.67	<u>63.08</u>	64.36
SKODA	17.76	<u>23.48</u>	22.52	25.56	11.64	<u>15.27</u>	14.69	16.94
UCI HAR	54.01	55.68	<u>57.69</u>	59.38	43.03	44.61	<u>45.54</u>	46.69
USCHAD	30.52	32.01	<u>34.69</u>	36.64	18.73	20.45	<u>22.14</u>	23.86
WISDM	54.61	55.74	<u>58.16</u>	61.25	37.56	38.23	<u>40.32</u>	42.67
Average	45.29	47.43	<u>48.83</u>	51.05	34.48	36.25	<u>37.15</u>	38.90

C. Model Analysis

1) Full Results on the Impact of Prototypes Numbers:

Analyzing Table IX, we observe that the number of prototypes significantly impacts model performance across the 91 UCR datasets. The model with 32 prototypes achieves the best average accuracy (67.78%) and highest number of best-performing cases (25 datasets), followed by the 64-prototype configuration (67.48% accuracy, 22 datasets). Both smaller (4 and 8 prototypes) and larger (64 prototypes) configurations show slightly decreased performance (67.15%, 67.16%, and 67.48% respectively), suggesting an optimal balance point around 32 prototypes.

Notably, some datasets show consistent improvement with increasing prototypes (e.g., FreezerRegularTrain: 85.06% → 91.35%), while others perform better with fewer prototypes (e.g., ItalyPowerDemand: 78.88% → 73.60%). This pattern indicates that different temporal patterns may require varying levels of prototype complexity for optimal representation. The balanced performance of the 32-prototype configuration across diverse datasets validates our design choice for prototype count, providing effective feature representation while maintaining computational efficiency.

TABLE VI

DETAILED PERFORMANCE COMPARISON OF VARIOUS METHODS ON UCR DATASETS. WE CALCULATE THE ACCURACY AND F1-SCORE (%) FOR EACH DATASET. **BLUE**: BEST RESULTS, **PURPLE**: SECOND BEST.

Datasets	Accuracy				Macro-F1			
	Sup.	Individual	Vanilla	ProtoN-FM	Sup.	Individual	Vanilla	ProtoN-FM
Adiac	34.70	33.42	52.86	54.99	23.38	22.83	39.88	41.59
AllGestureWiimoteX	46.38	49.19	48.29	49.90	13.31	14.99	13.52	14.22
AllGestureWiimoteY	50.43	53.95	53.33	53.10	13.84	14.43	14.35	14.39
AllGestureWiimoteZ	43.95	46.67	44.86	45.24	11.70	12.19	11.75	11.86
ArrowHead	46.86	44.00	56.57	56.95	26.74	21.58	28.05	30.69
Beef	33.33	32.22	44.44	53.33	25.90	27.62	43.24	53.25
BeetleFly	50.00	43.33	50.00	58.33	41.70	40.57	42.13	56.81
BirdChicken	63.33	48.33	85.00	73.33	61.30	45.37	84.89	70.63
BME	43.33	50.67	48.22	52.00	32.66	38.92	29.20	29.51
CBF	59.04	60.33	69.96	64.81	51.80	55.20	67.67	61.23
Chinatown	76.19	77.45	70.36	67.44	48.16	46.91	43.25	41.15
ChlorineConcentration	53.32	53.39	53.67	56.30	37.21	36.95	38.22	43.58
Coffee	90.48	92.86	76.19	75.00	90.43	92.45	75.64	74.59
CricketX	48.03	48.97	51.62	49.57	43.55	43.50	47.08	45.12
CricketY	41.88	40.43	46.07	44.79	35.92	34.63	39.91	37.69
CricketZ	49.57	42.31	50.09	52.99	44.14	37.68	43.00	47.31
Crop	54.07	56.54	58.28	59.85	16.47	16.86	19.79	21.14
DiatomSizeReduction	63.18	39.11	80.83	85.95	45.33	25.75	63.82	67.74
DistalPhalanxOutlineAgeGroup	73.38	73.38	73.38	73.14	59.28	61.73	61.97	60.49
DistalPhalanxOutlineCorrect	71.26	71.26	74.15	71.38	68.48	67.40	72.18	70.15
DistalPhalanxTW	64.99	65.47	66.91	66.19	44.09	40.43	47.72	45.64
DodgerLoopDay	27.08	36.25	35.42	33.75	15.20	21.18	19.86	19.97
DodgerLoopGame	56.04	57.49	52.90	50.72	37.75	40.07	36.37	35.92
DodgerLoopWeekend	69.32	74.88	77.54	80.43	43.91	47.84	50.05	54.76
Earthquakes	69.54	67.87	70.74	72.66	51.83	49.44	51.78	55.16
ECG200	80.67	80.67	84.67	87.67	77.07	77.52	81.74	86.25
ECG5000	92.68	92.21	92.61	93.34	68.72	69.83	70.24	72.40
ECGFiveDays	63.96	62.21	64.50	67.48	61.73	59.09	58.90	64.94
ElectricDevices	49.01	52.14	50.02	52.54	23.67	28.04	26.42	28.99
FaceAll	70.06	68.62	68.66	68.30	23.16	21.53	23.53	22.81
FaceFour	42.42	43.56	45.83	58.71	38.43	36.99	37.56	54.07
FacesUCR	59.92	58.54	65.51	66.50	48.99	47.24	54.46	55.61
FiftyWords	40.15	41.39	43.37	42.86	21.83	22.03	23.75	23.81
Fish	56.00	55.24	72.57	74.29	50.81	48.70	69.84	70.73
FordA	92.47	92.80	92.05	92.27	92.20	92.52	91.77	92.01
FordB	76.17	75.68	76.30	76.79	75.44	75.07	75.37	76.08
FreezerRegularTrain	75.16	75.61	86.92	90.02	43.20	43.39	48.99	55.88
FreezerSmallTrain	59.01	64.51	73.54	69.65	35.82	38.11	42.58	40.95
GestureMidAirD1	46.67	47.18	53.85	54.10	37.86	40.41	44.79	44.63
GestureMidAirD2	35.38	41.54	36.67	37.18	25.36	31.28	25.98	27.82
GestureMidAirD3	15.90	17.44	21.54	22.56	10.44	12.79	16.39	17.61
GesturePebbleZ1	69.57	67.25	66.47	66.86	62.82	59.26	60.43	60.84
GesturePebbleZ2	63.50	67.72	73.42	68.78	57.04	60.88	68.14	63.08
GunPoint	67.11	65.33	68.67	81.33	66.01	62.46	67.59	80.78
GunPointAgeSpan	74.58	77.43	86.92	88.71	42.30	43.21	49.72	50.30
GunPointMaleVersusFemale	81.86	83.33	82.91	83.33	48.26	48.89	48.54	48.76
GunPointOldVersusYoung	99.89	99.89	95.03	97.14	98.28	98.28	80.15	84.43
Ham	73.97	75.56	74.60	76.19	53.13	53.54	52.04	53.08
Herring	51.04	56.77	57.29	56.25	48.90	52.84	52.91	50.94
InsectWingbeatSound	39.93	39.44	43.42	44.49	34.77	33.87	38.23	39.28
ItalyPowerDemand	72.92	70.65	72.53	73.60	71.89	69.47	71.39	72.48
Lightning7	57.08	49.77	64.84	62.10	51.03	40.14	61.14	56.51
Meat	74.44	66.67	75.00	80.56	56.63	61.62	62.19	56.91
MedicalImages	62.54	64.52	64.34	62.41	50.49	47.39	53.52	47.86
MelbournePedestrian	87.67	88.26	88.34	88.33	46.96	48.06	44.25	45.79
MiddlePhalanxOutlineAgeGroup	56.28	59.52	54.55	59.09	39.32	40.59	39.71	37.72
MiddlePhalanxOutlineCorrect	54.07	51.32	75.37	76.75	40.74	40.33	73.41	74.16
MiddlePhalanxTW	55.19	53.90	56.71	54.33	30.67	31.89	37.02	34.93
MoteStrain	82.88	75.56	56.79	71.35	82.42	72.96	55.47	70.13
OSULeaf	57.99	59.92	63.77	64.60	53.87	56.06	60.11	59.05
PhalangesOutlinesCorrect	63.44	65.15	68.41	68.41	48.51	47.97	57.75	59.31
PickupGestureWiimoteZ	40.00	29.33	29.33	36.67	25.88	19.77	18.84	24.64
Plane	85.71	85.40	96.83	91.43	80.57	80.02	95.97	90.09
PowerCons	88.33	86.30	89.63	88.70	77.84	75.19	79.47	78.52
ProximalPhalanxOutlineAgeGroup	81.46	80.33	84.23	85.85	59.46	59.15	61.15	61.65
ProximalPhalanxOutlineCorrect	75.95	77.55	78.92	79.84	59.83	61.22	70.30	71.87
ProximalPhalanxTW	76.26	75.93	74.15	74.80	47.36	46.58	47.23	49.87
ShakeGestureWiimoteZ	43.33	44.67	70.67	66.00	30.90	31.99	54.91	51.23
ShapeletSim	48.33	50.19	73.52	71.67	33.79	34.77	46.71	45.42
ShapesAll	58.89	58.72	64.33	66.44	22.66	22.83	26.74	27.77
SmoothSubspace	96.44	96.22	95.33	94.89	84.42	80.64	79.94	77.46
SonyAIBORobotSurface1	47.37	45.04	80.53	72.32	39.15	38.55	79.97	71.03
SonyAIBORobotSurface2	68.80	68.98	61.32	67.05	64.47	65.62	58.94	60.45
Strawberry	93.33	90.90	93.33	93.33	80.72	76.45	80.82	86.02
SwedishLeaf	77.81	77.01	82.24	82.93	67.07	66.30	72.15	72.44
Symbols	27.47	25.96	33.07	34.51	17.07	16.26	25.77	25.75
SyntheticControl	94.33	94.22	95.44	94.78	66.68	71.88	66.27	67.28
ToeSegmentation1	66.81	55.85	62.13	74.42	43.09	37.40	40.33	46.04
ToeSegmentation2	50.26	50.77	57.95	69.49	35.30	35.91	38.91	44.27
Trace	70.67	73.00	87.00	89.33	65.51	68.89	86.20	88.69
TwoLeadECG	58.88	55.52	60.08	61.08	57.21	50.35	54.66	55.76
TwoPatterns	74.97	75.30	79.96	85.56	74.15	74.34	79.16	84.67
UMD	42.36	45.83	74.77	74.31	21.90	23.04	37.90	38.68
UWaveGestureLibraryX	65.87	63.51	66.02	67.97	61.61	59.13	62.28	63.14
UWaveGestureLibraryY	59.65	59.41	56.47	58.75	54.92	53.86	52.31	54.29
UWaveGestureLibraryZ	62.27	60.41	60.06	62.02	57.54	56.11	55.21	58.24
Wafer	96.80	97.22	97.84	97.77	90.58	91.07	93.18	92.80
Wine	50.00	50.00	69.14	62.96	41.54	41.54	50.66	44.83
WordSynonyms	31.56	30.46	37.72	37.10	14.04	12.04	20.77	20.65
Yoga	69.61	68.57	77.63	77.00	68.54	67.26	76.99	76.40
Average	62.03	61.53	66.66	67.78	48.30	47.65	52.50	53.51
1 st Count	11	16	28	42	9	17	24	41

TABLE VII
DETAILED COMPARISON OF MOMENT AND PROTON-FM PERFORMANCE ON 91 UCR DATASETS

Dataset	Accuracy (%)		Dataset	Accuracy (%)	
	MOMENT	ProtoN-FM		MOMENT	ProtoN-FM
GestureMidAirD2	36.1538	32.3077	PowerCons	68.3333	65.0000
UWaveGestureLibraryX	47.4037	47.4037	PhalangesOutlinesCorrect	63.5198	62.9371
GesturePebbleZ2	35.4430	36.7089	BirdChicken	85.0000	85.0000
ECG5000	90.6444	90.1778	ToeSegmentation2	73.8462	76.1538
OSULeaf	43.3884	40.9091	CricketY	33.5897	31.2821
MedicalImages	55.6579	55.1316	ElectricDevices	55.8034	55.8293
Ham	64.7619	64.7619	DodgerLoopGame	59.4203	63.7681
DistalPhalanxTW	64.0288	66.9065	Fungi	26.3441	31.1828
ProximalPhalanxOutlineCorrect	71.1340	68.7285	Symbols	49.7487	45.7286
FreezerRegularTrain	75.5789	75.7895	UWaveGestureLibraryZ	49.2183	50.1396
TwoLeadECG	67.4276	70.4126	ECG200	77.0000	77.0000
GunPointMaleVersusFemale	97.4684	97.7848	MoteStrain	76.1981	76.5176
Trace	71.0000	71.0000	Strawberry	64.3243	64.3243
SmoothSubspace	86.6667	88.6667	InsectWingbeatSound	24.1414	22.0202
MiddlePhalanxTW	58.4416	59.0909	DodgerLoopWeekend	81.1594	79.7101
SyntheticControl	89.6667	88.3333	Meat	56.6667	66.6667
ShapesAll	38.8333	40.6667	MelbournePedestrian	83.6818	80.6068
AllGestureWiimoteX	25.0000	23.0000	FaceAll	44.1420	43.4320
Wafer	89.2116	89.2116	FacesUCR	45.7073	41.0732
FaceFour	71.5909	70.4545	AllGestureWiimoteY	37.8571	36.7143
CricketX	35.1282	34.1026	ShakeGestureWiimoteZ	32.0000	32.0000
DistalPhalanxOutlineCorrect	67.3913	65.9420	BME	40.6667	35.3333
ChlorineConcentration	55.8594	55.7031	FordB	60.2469	59.1358
Chinatown	61.2245	60.9329	Fish	46.8571	50.2857
GestureMidAirD1	29.2308	26.9231	SonyAIBORobotSurface2	81.4271	83.0010
MiddlePhalanxOutlineAgeGroup	59.7403	59.7403	FiftyWords	33.4066	27.4725
UMD	47.9167	52.7778	ToeSegmentation1	66.2281	65.3509
Crop	59.4048	58.8274	FreezerSmallTrain	74.0000	77.8246
GesturePebbleZ1	32.5581	31.3953	TwoPatterns	51.8750	51.7750
WordSynonyms	28.9969	30.0940	ShapeletSim	70.5556	68.8889
ArrowHead	40.5714	53.7143	Plane	72.3810	72.3810
Wine	50.0000	50.0000	GestureMidAirD3	20.0000	20.7692
Coffee	64.2857	53.5714	DiatomSizeReduction	69.9346	78.4314
Earthquakes	74.8201	74.8201	CricketZ	33.0769	36.9231
Herring	59.3750	59.3750	Lightning7	52.0548	60.2740
Beef	43.3333	53.3333	UWaveGestureLibraryY	47.7945	48.3250
MiddlePhalanxOutlineCorrect	57.0447	57.0447	GunPointAgeSpan	73.7342	75.3165
ECGFiveDays	65.0406	66.7828	DistalPhalanxOutlineAgeGroup	69.0647	71.2230
Yoga	58.1333	61.6000	SwedishLeaf	57.6000	58.2400
Adiac	10.9974	13.0435	CBF	60.0000	61.7778
AllGestureWiimoteZ	18.0000	20.7143	BeetleFly	70.0000	65.0000
DodgerLoopDay	31.2500	40.0000	GunPointOldVersusYoung	74.6032	75.8730
FordA	75.7576	75.3030	ItalyPowerDemand	95.4325	94.2663
ProximalPhalanxOutlineAgeGroup	83.9024	84.3902	GunPoint	62.0000	66.6667
ProximalPhalanxTW	80.0000	78.5366	PickupGestureWiimoteZ	36.0000	36.0000
SonyAIBORobotSurface1	74.5424	79.2013			
Average				57.6994	58.2740
1 st Count				55 / 91	

TABLE VIII
DETAILED COMPARISON OF MOIRAI AND PROTON-FM ON MONASH TIME SERIES FORECASTING BENCHMARK

Dataset	Moirai	ProtoN-FM	Dataset	Moirai	ProtoN-FM
australian_electricity	295.0703	238.8042	m4_monthly	605.0799	592.0217
bitcoin_with_missing	1.38E+16	1.73E+16	m4_weekly	351.9710	351.7271
car_parts_with_missing	0.4716	0.4643	monash_m3_monthly	696.5747	702.7923
cif_2016	394655.1680	359786.3691	monash_m3_other	308.2975	231.8303
covid_deaths	140.3132	150.0006	nn5_daily_missing	4.7384	4.4790
fred_md	6556.7734	4212.2568	nn5_weekly	14.9696	15.3427
hospital	20.8099	22.8997	pedestrian_counts	57.0090	55.1129
kdd_cup_2018	39.4536	38.9629	rideshare_missing	1.1888	1.1850
m1_monthly	2210.0315	2025.3065	saugeenday	23.9684	24.0972
m4_daily	188.7526	185.3714	sunspot_missing	2.2522	0.1507
m4_hourly	288.3103	251.0390	temp_rain_missing	5.1228	4.9981
tourism_monthly	3295.9609	3386.3516	traffic_hourly	0.0173	0.0166
tourism_quarterly	15973.7295	13781.4639	traffic_weekly	1.1617	1.1528
us_births	690.9827	570.3322	weather	1.8925	1.8660
Summary Statistics					
Normalized MAE	Moirai	ProtoN-FM	1 st Count	Moirai	ProtoN-FM
	1.00	0.8893		7	21

TABLE IX

DETAILED ACCURACY RESULTS (%) ON UCR ARCHIVE USING VARYING NUMBER OF PROTOTYPES. **BLUE**: BEST RESULTS, **PURPLE**: SECOND BEST.

Dataset	ProtoN4-FM	ProtoN8-FM	ProtoN16-FM	ProtoN32-FM	ProtoN64-FM
Adiac	57.20	56.01	53.71	54.99	52.86
AllGestureWiimoteX	50.76	50.67	48.81	49.90	50.38
AllGestureWiimoteY	53.29	54.24	53.95	53.10	53.24
AllGestureWiimoteZ	43.95	44.81	44.19	45.24	45.10
ArrowHead	54.86	56.19	50.29	56.95	57.71
Beef	46.67	42.22	46.67	53.33	48.89
BeetleFly	55.00	65.00	50.00	58.33	53.33
BirdChicken	66.67	65.00	71.67	73.33	83.33
BME	55.33	53.11	43.11	52.00	49.11
CBF	69.26	68.89	66.44	64.81	65.96
Chinatown	67.83	69.00	70.36	67.44	69.39
ChlorineConcentration	56.63	48.85	53.29	56.30	52.16
Coffee	78.57	75.00	75.00	75.00	73.81
CricketX	48.72	51.45	50.26	49.57	52.48
CricketY	43.59	46.24	46.07	44.79	48.72
CricketZ	49.83	50.94	51.45	52.99	51.88
Crop	59.01	59.35	59.87	59.85	59.10
DiatomSizeReduction	86.82	85.51	86.60	85.95	85.84
DistalPhalanxOutlineAgeGroup	74.82	74.82	75.78	73.14	73.14
DistalPhalanxOutlineCorrect	75.36	75.36	72.95	71.38	75.97
DistalPhalanxTW	67.39	65.23	67.63	66.19	63.07
DodgerLoopDay	39.58	40.42	36.67	33.75	38.75
DodgerLoopGame	51.69	53.38	57.00	50.72	53.14
DodgerLoopWeekend	85.27	87.20	85.27	80.43	88.65
Earthquakes	74.10	73.38	70.74	72.66	69.78
ECG200	84.33	83.00	86.33	87.67	83.33
ECG5000	93.09	92.39	92.71	93.34	92.39
ECGFiveDays	66.01	67.40	66.82	67.48	66.67
ElectricDevices	51.71	53.72	48.80	52.54	52.20
FaceAll	66.69	68.32	68.88	68.30	62.82
FaceFour	50.38	49.24	52.65	58.71	53.79
FacesUCR	64.59	65.61	67.24	66.50	65.85
FiftyWords	43.37	41.10	43.74	42.86	41.25
Fish	74.67	71.62	74.67	74.29	71.62
FordA	92.58	92.93	92.17	92.27	91.74
FordB	76.21	76.63	76.58	76.79	76.63
FreezerRegularTrain	85.06	85.12	87.49	90.02	91.35
FreezerSmallTrain	71.68	73.64	73.60	69.65	71.37
GestureMidAirD1	51.54	52.82	50.51	54.10	50.51
GestureMidAirD2	37.69	36.67	41.28	37.18	37.44
GestureMidAirD3	21.03	22.56	22.82	22.56	23.08
GesturePebbleZ1	64.92	63.18	67.44	66.86	67.64
GesturePebbleZ2	70.04	67.93	69.41	68.78	73.63
GunPoint	70.44	76.89	81.33	81.33	78.44
GunPointAgeSpan	88.29	85.65	86.29	88.71	89.45
GunPointMaleVersusFemale	81.22	83.12	83.33	83.33	83.23
GunPointOldVersusYoung	95.24	97.25	99.26	97.14	94.39
Ham	73.33	75.24	76.51	76.19	74.92
Herring	58.33	58.85	59.38	56.25	60.42
InsectWingbeatSound	43.59	42.14	42.61	44.49	43.30
ItalyPowerDemand	78.88	78.78	76.19	73.60	77.19
Lightning7	62.10	60.73	60.27	62.10	62.10
Meat	76.67	78.33	80.00	80.56	80.56
MedicalImages	63.33	60.09	63.77	62.41	64.39
MelbournePedestrian	89.72	88.89	89.11	88.33	88.88
MiddlePhalanxOutlineAgeGroup	58.44	55.41	56.28	59.09	56.28
MiddlePhalanxOutlineCorrect	76.86	73.88	76.40	76.75	76.86
MiddlePhalanxTW	52.60	52.60	56.71	54.33	53.90
MoteStrain	63.45	66.77	66.13	71.35	70.15
OSULeaf	65.15	63.09	65.56	64.60	65.29
PhalangesOutlinesCorrect	69.31	70.98	68.22	68.41	66.98
PickupGestureWiimoteZ	36.67	35.33	36.00	36.67	30.67
Plane	91.43	90.16	92.70	91.43	90.79
PowerCons	90.56	90.19	90.37	88.70	89.63
ProximalPhalanxOutlineAgeGroup	85.37	85.37	83.74	85.85	86.67
ProximalPhalanxOutlineCorrect	79.61	78.47	78.92	79.84	77.78
ProximalPhalanxTW	76.10	74.15	72.68	74.80	78.05
ShakeGestureWiimoteZ	65.33	64.00	65.33	66.00	68.67
ShapeletSim	77.41	63.52	73.15	71.67	70.93
ShapesAll	67.00	66.11	65.28	66.44	65.44
SmoothSubspace	95.56	95.11	95.11	94.89	95.11
SonyAIBORobotSurface1	75.10	69.83	68.28	72.32	75.93
SonyAIBORobotSurface2	65.72	65.65	65.90	67.05	65.97
Strawberry	94.14	92.52	93.24	93.33	93.60
SwedishLeaf	81.60	80.91	85.01	82.93	82.93
Symbols	34.27	32.96	35.11	34.51	35.08
SyntheticControl	94.89	95.89	95.67	94.78	94.44
ToeSegmentation1	76.61	81.14	81.58	74.42	56.87
ToeSegmentation2	63.33	69.23	61.54	69.49	66.92
Trace	90.33	86.67	88.67	89.33	91.67
TwoLeadECG	53.38	60.90	61.02	61.08	61.93
TwoPatterns	86.75	88.61	87.58	85.56	87.08
UMD	68.29	71.99	67.59	74.31	74.07
UWaveGestureLibraryX	66.83	67.18	66.42	67.97	67.59
UWaveGestureLibraryY	57.44	58.96	58.19	58.75	58.33
UWaveGestureLibraryZ	62.14	63.34	60.91	62.02	60.84
Wafer	97.46	97.54	97.28	97.77	97.30
Wine	51.85	58.64	61.11	62.96	59.88
WordSynonyms	35.37	36.57	36.94	37.10	36.52
Yoga	78.28	79.02	77.67	77.00	76.33
Average	67.15	67.16	67.35	67.78	67.48
1st Count	19	12	20	25	22